Received: 2 January 2019 | Revised: 5 March 2019 | Accepted: 22 April 2019

DOI: 10.1002/aoc.5011

WILEY Applied Organometallic Chemistry

FULL PAPER

Hexanuclear Zn(II) and Mononuclear Cu(II) Complexes containing imino phenol ligands: Exploitation of their Catalytic and Biological Perspectives

Shyam Sundar Mondal[1] | Manosree Chatterjee[2] | Ranjay K. Tiwari[3,4] | J.N. Behera[3,4] | Nripen Chanda[2] | Sourav Biswas[1] | Tanmoy Kumar Saha[1]

[1]Department of Chemistry, National Institute of Technology Durgapur, West Bengal, India, 713209

[2]Department of Materials Processing and Microsystems Laboratory, CSIR-Central Mechanical Engineering Research Institute, West Bengal, India, 713209

[3]Department of Chemistry, National Institute of Science Education and Research, Bhubaneswar, Odisha, India, 752050

[4]Homi Bhabha National Institute, Mumbai, India, 400094

Correspondence
Tanmoy Kumar Saha, Department of Chemistry, National Institute of Technology Durgapur. West Bengal, India-713209.
Email: chem.tanmoy@gmail.com

Funding information
Science and Engineering Research Board, Grant/Award Number: ECR/2016/000681

A unique hexanuclear zinc(II) (**1**) and two mononuclear copper(II) (**2** and **3**) complexes anchored with imino phenol ligand $\mathbf{HL^1}$ and $\mathbf{HL^2}$ were synthesized with good yield and purity (where $\mathbf{HL^1}$ = 4-*tert*-butyl-2,6-bis((mesitylimino) methylphenol and $\mathbf{HL^2}$ = 5-*tert*-butyl-2-hydroxy-3-((mesitylimino)methyl) benzaldehyde). These complexes were characterized by utilizing various spectroscopic protocols like NMR, FTIR, UV as well as ESI-Mass spectrometry, elemental analysis and single crystal X-ray diffraction studies. Their potential to bind calf thymus DNA (CT-DNA) was tested utilizing different techniques such as UV–visible and fluorescence spectroscopy. The experiment implies that they interact with CT-DNA *via* non-intercalative mode with moderate capabilities ($K_b \sim 10^4\ M^{-1}$). On the other hand, these complexes have high capabilities to quench the fluorescence of bovine serum albumin (BSA) following the static pathway. In addition, they are active catalysts for the oxidation reaction of 3,5-di-*tert*-butylcatechol (3,5-DTBC) to 3,5-di-*tert*-butylquinone (3,5-DTBQ) under aerobic condition. From the recorded EPR signals of all complexes, it has been concluded that the oxidation reaction proceeds *via* ligand oriented radical pathway instead of metal based redox participation. Kinetic studies using **1–3** indicate that it follows Michaelis–Menten type of equation with moderate to high turnover number (k_{cat}). Apart from these aspects, complexes **1–3** were screened for their cytotoxic behavior towards HeLa cells (human cervical carcinoma) and found quite active with comparable IC_{50} values to cisplatin.

KEYWORDS
catecholase activity, cytotoxic activity, DNA and protein binding, Hexanuclear zinc (II) complex, mononuclear copper (II) complex

1 | INTRODUCTION

Schiff base ligand is one of the most promising candidates in coordination chemistry with different denticities in terms of complex formation with metal ions. In the recent era, great blooming has been observed on the development of Schiff base ligands containing diversified organic scaffolds. The interest has been manifested due to their ease of preparation and formation of stable coordination complexes with most of the transition metals. In these

complexes, variable coordination number, oxidation states of metal ion, type of the attached ligand, kinetic and thermodynamic prospects do offer the active impetus to exploit a wide range of pharmaceutical and biological domains.[1–11] They also have enormous potential to create versatile platforms for rational strategies of drug design.

Cisplatin which is a most popular choice to treat cancer brings the metallodrugs in the frontline area against this threat since its discovery.[12–14] Nevertheless, the scope of Pt based drugs is still restricted owing to their toxic side effects[15] and drug resistance phenomena.[16–19] So, the researchers are keener to develop safe and efficacious anticancer drugs based on endogenous metals with superior pharmacological aspects. Now, the metal complexes can target DNA either by the covalent mode or non-covalent interactions. In the covalent mode, a nitrogen base of DNA residue (for example guanine N7) binds to the complex by replacing the labile ligand present in it.[9,20] In contrary, the non-covalent interaction involves intercalation, electrostatic effects and groove binding. Intercalation associates with the π–π stacking due to the partial insertion of aromatic rings present in ligand moiety between twin helical strands of DNA. Besides, the groove and electrostatic bindings associate the involvement of a metal complex by accessing the bases near to the edges of the DNA helix within the major or minor groove. In this context, copper and zinc based complexes have portrayed promising perspectives amongst many bio-compatible metals.

Copper is an extremely important microelement for living organisms and plays a pivotal role in the proper function of many metalloenzymes like cytochrome oxidase, tyrosinase, dopamine β-hydroxylase and superoxide dismutase.[21] It is also noteworthy that copper (II) based complexes have been widely exploited in DNA cleavage due to the production of reactive oxygen species (ROS) *via* the redox activity of copper ions. This enables it to attack at the different sites of DNA leading to rupture of double-strand.[22] Due to the apparent permeability of copper compounds through the membrane of a cancer cell, it accumulates in the targeted tumor. In recent times, a series of copper complexes are found active as potent drugs towards the anticancer activity both *in vitro* and *in vivo*.[9,10,22–27]

After iron, zinc is a vital trace element for the proper functioning of various biological processes[28] and is engrossed in the prodigious number of enzymes in mammalians. In the current era, Zn (II) complexes have grabbed tremendous attention due to their multidimensional aspects in many research areas.[29–36] Current investigations have depicted that these compounds are proven to be active in medicinal therapeutic uses,[37,38] in particular for the treatment of cancer with low *in vivo* toxicity and reduced side effects.[29,39–46]

Now, the phenolic Schiff base ligands with nitrogen and oxygen atoms as donor centers have flexible coordinating characters along with hard and relatively softer sites. Nonetheless, copper and zinc ions have remarkable affinity to bind with these types of Schiff base ligands through chelation.[47–49] In past decades, transition metal complexes comprising of phenolic moieties in the ligand skeleton were reported owing to their appreciable binding and cleaving abilities towards DNA.[3,29,50–52]

All these above facts encouraged us to investigate the catalytic and biological activities of a unique hexanuclear Zn(II) and two mononuclear Cu(II) complexes having imino phenolate ligand. Copper and zinc were selected for coordination due to their biocompatibility, effectiveness in the bio-medical field and low toxicity compared to the conventional Pt based drugs. Therefore, we report the synthesis, structural characterization of hexanuclear zinc(II) and two mononuclear copper(II) complexes consisting of *tert*-butyl((mesitylimino)methyl)phenol ligand units (**HL$^{1-2}$**) (Scheme 1). The potential of these complexes was investigated towards the DNA binding, protein binding, catecholase and cytotoxic activities. Moreover, this is the first example in the literature of such hexanuclear Zn(II) complex as per our knowledge whose catecholase and cytotoxic activities were studied.

2 | EXPERIMENTAL

2.1 | General information and instrumentation

All the reagents and chemicals were purchased from commercial sources and used without further purification. Solvents were dried and purified according to

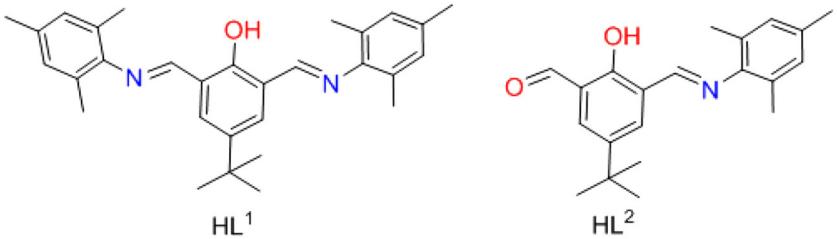

SCHEME 1 *tert*-Butyl((mesitylimino)methyl)phenol ligand used for complex formation

standard procedure prior to use. 3,5-di-*tert*-butylcatechol (3,5-DTBC), Ethidium bromide (EB), 3-(4,5-dimethylthiazol-2-yl)-2,5-diphenyltetrazolium bromide (MTT), bovine serum albumin (BSA) and calf thymus DNA (CT-DNA) were obtained from Sigma. The Tris–HCl buffer solution was prepared with double-distilled water.

Elemental analysis (% CHN) was performed using a Thermo Fisher Flash 2000 CHNS funded by DST-FIST grant, Govt. of India. Infrared (IR) spectra were recorded using KBr pellet method in the range 4000–400 cm^{-1} with a Bruker Alpha FTIR spectrometer. Electronic spectra were recorded using a Shimadzu UV-1800 spectrophotometer in the range 200–800 nm. Fluorescence emission spectra were measured using a Hitachi F-2500 spectrofluorometer using a 1.0 cm quartz cell. The ^{1}H and ^{13}C NMR spectra of the zinc (II) complex were collected on a Bruker Avance 400 spectrometer in $CDCl_3$ at room temperature. EPR Spectra were recorded on a Magnettech MS-5000 by Freiberg Instruments, Germany.

2.2 | Synthesis of Schiff base ligand

The ligand **HL^1**, 4-*tert*-butyl-2,6-bis((mesitylimino) methyl)phenol, was prepared from 4-*tert*-butyl-2,6-diformyl phenol and 2,4,6-trimethyl aniline according to reported literature method.[53]

2.3 | Synthesis of metal complexes

2.3.1 | Complex 1

To a stirred acetonitrile solution of **HL^1** (0.044 g, 0.1 mmol), ethanolic solution of $Zn(OAc)_2{\cdot}2H_2O$ (0.066 g, 0.3 mmol) was added drop wise for a period of 15 mins. Then, the resulting solution was refluxed for 12 hr under N_2 atmosphere. The resulting light yellow color solution was kept at room temperature for crystallization. After one week, square shape light yellow crystals were obtained. Yield: 0.150 g (85%). Anal. Calc. for $C_{76}H_{94}N_4O_{20}Zn_6$: C, 51.39; H, 5.44; N, 3.12. Found: C; 51.79; H; 5.60; N; 3.15. IR (KBr): 2960(m, $\nu_{C\text{-}H}$), 2916(w, $\nu_{C\text{-}H}$), 2862(w, $\nu_{C\text{-}H}$), 1613(s, $\nu_{C=N}$), 1592(s, $\nu_{C=C}$), 1536(s, $\nu_{asym\text{-}COO}$), 1478(m, $\nu_{C=C}$), 1437(s, $\nu_{sym\text{-}COO}$), 1196(s, $\nu_{phenolic\text{-}C\text{-}O}$). ^{1}H NMR ($CDCl_3$, 400 MHz): 1.27 (s, CO–CH_3, 6H), 1.34 (s, C (CH_3)$_3$, 18H), 2.11 (s, Ar–CH_3, 12H), 2.14–2.16 (s, Ar–CH_3, 24H), 2.17–2.30 (s, H_3C–C(–O–)$_2$, 18H), 6.76 (s, Ar–*H*, 2H), 6.89–6.93 (s, Ar–*H*, 8H), 7.41 (s, Ar–*H*, 2H), 8.15 (s, C*H*=N, 2H), 8.38 (s, C*H*=N, 2H).^{13}C NMR ($CDCl_3$, 100 MHz): 18.30 (C (CH_3)$_3$), 20.73 (H_3C–C(–O–)$_2$), 20.79 (H_3C–*C*(–O–)$_2$), 23.20 (Ar–*C*H_3), 30.90 (Ar–*C*H_3), 31.26 (*C* (CH_3)$_3$), 121.08 (Ar–*C*), 121.88 (Ar–*C*), 123.88 (Ar–*C*), 128.24 (Ar–*C*), 128.83 (Ar–*C*), 129.16 (Ar–*C*), 129.36 (Ar–*C*), 129.84 (Ar–*C*), 134.95 (Ar–*C*), 135.09 (Ar–*C*), 139.18 (Ar–*C*), 141.74 (*Ar*–O), 166.30 (*C*=N), 173.20 (O–*C* (CH_3)–O), 174.53 (O–*C* (CH_3)–O), 181.16 (O–*C* (CH_3)–O), 206.89 (*C*=O). ESI *m/z* calculated for $[M]^+$; $C_{76}H_{94}N_4O_{20}Zn_6$: 1774.08 found 1774.45.

2.3.2 | Complex 2

To a stirred solution of **HL^1** (0.088 g, 0.2 mmol) in 10 ml toluene was combined with a solution of $Cu(OAc)_2{\cdot}H_2O$ (0.018 g, 0.1 mmol) in 5 ml toluene. Then the resultant mixture was refluxed for 12 hr at 112 °C under N_2 atm. The resulting deep green color solution was kept for slow evaporation. After few days, block shape crystals were formed suitable for single crystal X-ray diffraction. Yield: 0.078 g (83%). Anal. Calc. for $C_{60}H_{70}CuN_4O_2$: C, 76.44; H, 7.48; N, 5.94. Found: C, 76.64; H, 7.53; N, 6.02. IR (KBr pellets, cm^{-1}): 2963(m, $\nu_{C\text{-}H}$), 2911(w, $\nu_{C\text{-}H}$), 2856(w, $\nu_{C\text{-}H}$), 1624(s, $\nu_{C=N}$), 1615(s, $\nu_{C=N}$), 1591(s, $\nu_{C=C}$), 1193(s, $\nu_{phenolic\text{-}C\text{-}O}$). ESI *m/z* calculated for $[M + H]^+$; $C_{60}H_{70}N_4O_2Cu$: 942.76 found 943.49.

2.3.3 | Complex 3

An ethanolic solution (7 ml) of 2, 4, 6-trimethyl aniline (0.135 g, 1 mmol) was added very slowly to an ethanolic solution (11 ml) of 4-*tert*-butyl-2,6-diformyl phenol (0.206 g, 1 mmol) and the mixture was refluxed for 1 hr. Then, a methanolic solution (10 ml) of $Cu(OAc)_2{\cdot}H_2O$ (0.090 g, 0.5 mmol) was added and stirred for additional 3–4 hr. The whole experiment was performed under N_2 atm. The resulting solution was kept for slow evaporation. Yield: 0.488 g (69%). Anal. Calc. for $C_{42}H_{48}N_2O_4Cu$: C, 71.24; H, 6.79; N, 3.91; Found: C, 71.15; H, 6.89; N, 3.67. IR (KBr pellets, cm^{-1}): 2962(m, $\nu_{C\text{-}H}$), 2912(w, $\nu_{C\text{-}H}$), 2859(w, $\nu_{C\text{-}H}$), 1670(s, $\nu_{C=O}$), 1618(s, $\nu_{C=N}$), 1592(m, $\nu_{C=C}$), 1196(m, $\nu_{phenolic\text{-}C\text{-}O}$). ESI *m/z* calculated for $[M]^+$; $C_{42}H_{48}N_2O_4Cu$: 708.38 found 708.31.

2.4 | X-ray crystallography

Suitable single crystals of zinc (II) and copper (II) complexes (**1, 2** and **3)** were carefully chosen under a polarizing microscope and mounted at the tip of the thin glass fiber using cyanoacrylate adhesive. Single crystal structure determination was carried out on a Bruker AXS KAPPA-APEX II diffractometer equipped with a normal focus, 2.4 kW sealed-tube X-ray source (Mo-Kα radiation, λ = 0.71073 Å) operating at 50 kV and 30 mA and data was collected at 100 K. SAINT program used for the

integration and scaling of data. The corresponding structures were solved by the direct method using SHELXT-2014 and refined on F^2 by a full-matrix least-squares technique using the SHELXL-2014 program's package. An empirical absorption correction based on symmetry equivalent reflections was applied using SADABS.[54] The graphic programs DIAMOND[55] and ORTEP[56] were utilized to illustrate the structures. Non-hydrogen atoms were refined anisotropically. In the refinement, hydrogens were treated as riding atoms using the SHELXL default parameters. The hydrogen atoms were situated in the Fourier map and were refined with bond length restraints. In case of **2,** the solvent molecule having highest Q peak of electron density 1.62 situated near to C17 (distance between C17 and Q peak is 3.308 Å) was masked in olex2[57] software. The CCDC reference numbers of complexes **1–3** are 1852303, 1852304 and 1852305 respectively.

2.5 | DNA binding studies

2.5.1 | Absorption spectral titration

The binding interaction between all the complexes and CT-DNA was investigated by means of electronic absorption spectroscopy. At ambient temperature, the absorption band of CT-DNA at 260 and 280 nm in 5 mM Tris–HCl/50 mM NaCl buffer (pH = 7.2) solution produces a ratio of 1.8–1.9, signifying that the DNA was sufficiently free from proteins.[58] The stock solutions of CT-DNA were prepared in Tris- HCl/NaCl buffer and stored at 4 °C for less than 4 days. The concentration of DNA per nucleotide phosphate was ascertained by using its absorption intensity at 260 nm taking the molar absorption coefficient of 6600 M^{-1} cm^{-1}.[59a] The experiments were executed by keeping the complex concentration (50 μM) constant and varying CT-DNA concentration (0–50 μM). The complex-DNA solutions were incubated for 10 min at room temperature before the actual measurement. An equal quantity of CT-DNA solution was mixed to both cuvettes for eliminating the absorbance of CT-DNA itself. The intrinsic binding constant K_b can be found out using the following equation:

$$[\mathrm{DNA}]/(\varepsilon_a - \varepsilon_f) = [\mathrm{DNA}]/(\varepsilon_b - \varepsilon_f) + 1/K_b\,(\varepsilon_b - \varepsilon_f) \quad (1)$$

Where ε_a, ε_f, and ε_b correspond to A_{obs}/[Complex], the extinction coefficient for the free copper complex, and the extinction coefficient for the copper complex in the fully bound form respectively. A plot of [DNA]/ $(\varepsilon_a - \varepsilon_f)$ *vs.* [DNA] provides K_b as the ratio of the slope to the intercept.

2.5.2 | Ethidium bromide experiment

The ethidium bromide (EB) fluorescence experiment was performed in Tris–HCl/NaCl buffer (5 mM Tris–HCl, 50 mM NaCl, pH = 7.2). The solutions of all complexes were titrated into the prepared EB-DNA solution (9.75×10^{-5} M EB and 9.75×10^{-5} M CT-DNA). Fluorescence quenching was monitored *via* recording the change of fluorescence emission spectra at various complex concentrations (0–50 μM). The said samples were excited at 510 nm and emission was documented from 520 to 700 nm.

2.6 | BSA binding studies

A stock solution of BSA was made in phosphate buffer solution (pH = 7.4) and it was preserved in the dark at 4 °C for 24 hr. The exact concentration of the stock solution was ascertained spectroscopically following Bouguer–Lambert–Beer law. The preparation of stock solutions of complexes was done in DMF. Fluorescence quenching experiments were performed by keeping constant concentration of BSA (10 μM) and increasing concentrations of the aforementioned complexes (0–50 μM) at room temperature. After addition of the complex, the system was equilibrated for 10 min prior to the recording of spectra. These were measured at an excitation wavelength of 296 nm and the emission spectra from 300 to 500 nm.

2.7 | Cell culture

Human cervical carcinoma cell lines (HeLa) were acquired from the National Centre for Cell Science (NCCS), Pune, India. The cells were cultured in DMEM medium supplemented with 100 units ml^{-1} penicillin, 10% fetal bovine serum (FBS), and 100 μg ml^{-1} streptomycin. The cells were incubated maintaining a humidified atmosphere having 5% CO_2 at 37 °C. For the cytotoxic activities 3.5 mg of all the complexes were dissolved in 1 ml DMSO and then further diluted it in complete cultural media. In all the experiments, the percentage of DMSO was kept within 0.1–1%. DMSO was non-toxic to the cells upto 1% concentration.

2.7.1 | MTT assay

Complex actuated cytotoxicity experiments were done by using MTT assay method in 96-well microplates. HeLa cells were seeded into 96-well plates at a density of 1.5×10^4 cells/well. Different concentrations of

complexes (4.26–40.38 μg ml^{-1}) were added to the cells after overnight preincubation at 37 °C. Untreated cells were taken as control. After 48 hr of incubation, a freshly prepared MTT solution (5 mg mL^{-1}) in PBS buffer was mixed to each well and incubated again at 37 °C for 4 hr. Then, the concerned media were removed and the formed formazan crystals were then dissolved in 50 μL of DMSO. The absorbance was measured at 570 nm by a multi-well plate reader (Thermo Scientific Multiskan FC). The experiment was performed in triplicate and the percentage of cell viability was calculated using the following equation:

$$\text{Cell viability } (\%) = [A_{570}\ (\text{sample})/A_{570}\ (\text{control})] \times 100\%.$$

Where A_{570} (sample) indicates the reading from the wells after the treatment with metal complexes and A_{570} (control) corresponding to that from the wells with medium containing 10% FBS only.[59b]

The sensitivity of the cancer cells upon addition of the complexes was expressed in terms of IC_{50} value.

2.7.2 | Analysis of cell death

HeLa cells were cultured on two 35 mm cell culture petri dishes (1x10^5 cells/dish) until it reaches 50% confluency. The culture media was then replaced with serum-free media and incubated for 2 hr to attain synchronised cell cycle. Cells in one tissue culture dish were treated with 40.38 μg/ml of complex **1** and the other was maintained as control. Images were acquired at 1 hr interval with EVOS FL (Life Technologies) inverted fluorescence microscope. The blebbing of plasma membrane was examined after 10 hr. Next, Hoechst 33342 (Sigma Aldrich) staining was carried out once the prominent deformation in cell membrane was observed. After the treatment, the cells were washed with PBS buffer for 5 min at room temperature followed by fixation with 4% paraformaldehyde for 15 min. Cells were washed thrice with the same buffer followed by incubation with Hoechst 33342 (1 μg/ml) for 15 min in dark. After the staining, one time washing with PBS buffer was done and the plates were allowed to dry for 2 h. Images were obtained in fluorescent mode of EVOS FL (Life Technologies) inverted fluorescence microscope and the image analysis was carried out in PhotoScape software.

3 | RESULTS AND DISCUSSION

3.1 | Synthesis and characterization

Complex **1** and **2** have been synthesized by reacting the symmetrical ligand, $\mathbf{HL^1}$ with $Zn(OAc)_2{\cdot}2H_2O$ or $Cu(OAc)_2{\cdot}H_2O$ maintaining the corresponding molar ratio in a suitable solvent (Scheme 2). However, **3** was synthesized by the reaction of *in situ* obtained unsymmetrical ligand, $\mathbf{HL^2}$ with $Cu(OAc)_2{\cdot}H_2O$ in a 2:1 molar ratio (Scheme 3). Interestingly, it is quite tricky to have complex **3** due to the high chance of double condensed $\mathbf{HL^1}$ formation during the reaction instead of $\mathbf{HL^2}$. Careful trapping of the formed $\mathbf{HL^2}$ as Cu(II) complex by the

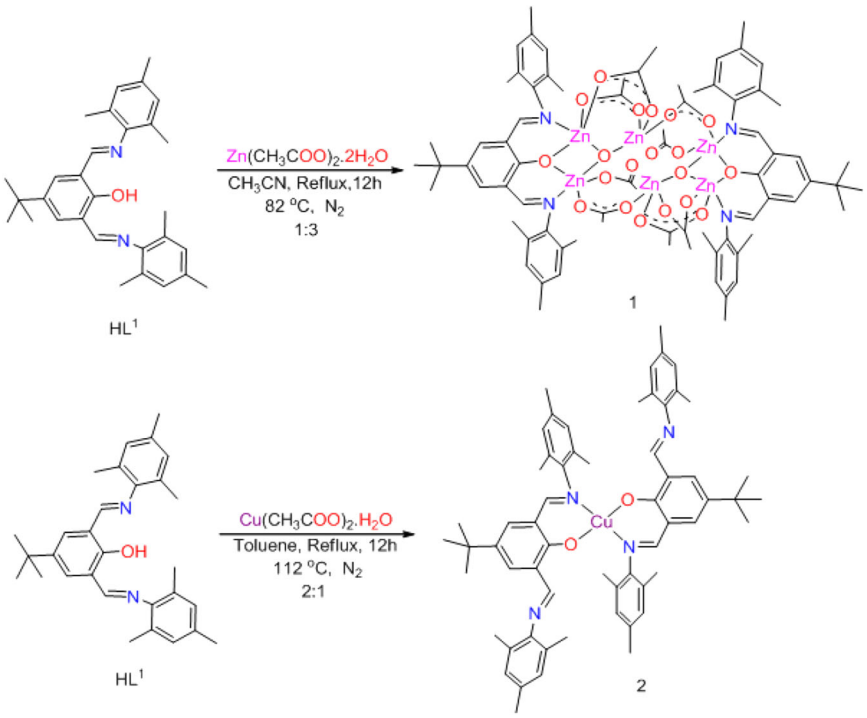

SCHEME 2 Synthesis of hexanuclear Zn(II) (**1**) and mononuclear Cu(II) (**2**) complexes comprising of $\mathbf{L^1}$ moieties

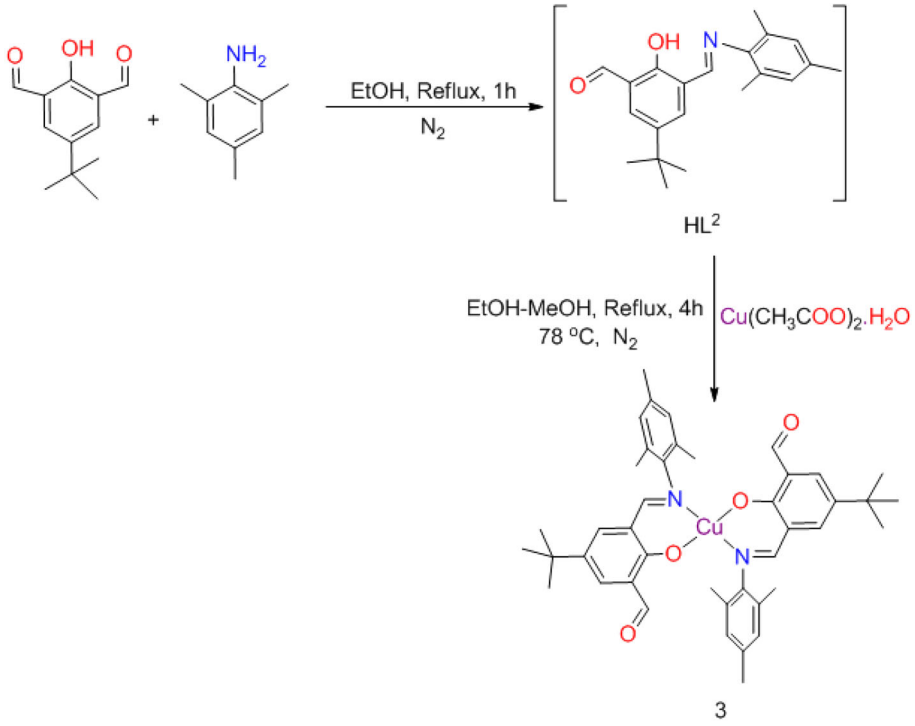

SCHEME 3 Synthesis of mononuclear Cu(II) complex (**3**) containing $\mathbf{L^2}$ unit

addition (after 1 hr) of $Cu(OAc)_2{\cdot}H_2O$ to the resultant solution of $\mathbf{HL^2}$ is the most suitable way to avoid the second condensation. However, similar efforts have been made to prepare a mono-condensed Zn(II) compound under the same reaction conditions. Surprisingly, we were unable to isolate the desired compound as the yield was very poor along with unidentified side products. Complexes **1**–**3** have been characterized by using modern spectroscopic techniques. Additionally, these compounds are structurally ascertained by single crystal X-ray diffraction studies.

To check the coordination behavior of the ligand in the synthesized complexes, IR spectra are recorded and compared with the free ligand. It has been observed that complexes **1**–**3** depict bands in the range of 1618–1613 cm^{-1} owing to the stretching of C=N of ligand moiety. The C=N stretching comes at a lower frequency in the complex in comparison with the free ligand ($\nu_{C=N}$ = 1631 cm^{-1}) due to the weakening of double bond character of C=N. This attributes the formation of the coordination bond to the metal ion through the nitrogen atom of imine moiety. Additionally, all the complexes show bands in the range of 2963–2856 cm^{-1} due to the aliphatic C–H stretching of the *tert*-butyl group. For complex **1**, the $\nu_{asymmetric}$ and $\nu_{symmetric}$ –COO of the acetate group appear at 1536 and 1437 cm^{-1} suggesting the bridging mode of acetate unit. Whereas, two sharp peaks appear at 1624 and 1615 cm^{-1} in complex **2** due to the non-coordinated and coordinated –C=N moieties. This was further confirmed by single crystal X-ray diffraction studies. On the other hand, a strong band near about 1670 cm^{-1} is present in case of **3** which is actually due to the free –C=O group attached to ligand part.

The molecular ion peak in electrospray ionization mass spectrometry (ESI–MS) of complexes **1**–**3** proves the existence of hexanuclear (for **1**) and mononuclear (for **2** and **3**) states for the metal ion in the corresponding compounds (See Supporting Information†). Elemental analysis results of **1**–**3** do exhibit considerable extent of purity for these compounds.

3.2 | Single crystal X-ray diffraction studies

The crystal data and refinement parameters for **1**, **2** and **3** have been summarized in Table 1. From single crystal X-ray diffraction studies, it is evident that complex **1** (Figure 1) is having a hexanuclear structure in the solid state and crystallizes in triclinic system with *P*-1 space group. It consists of six Zn(II) ions and two ligand moieties with several bridging and terminal acetate units. More interestingly, four Zn(II) ions (namely Zn1 and Zn2) in the complex are pentacoordinated with distorted square pyramidal geometry and the other two Zn3 ions are tetracoordinated with slightly distorted tetrahedron ascertained from the measured bond angles and bond distances. The ligand $\mathbf{HL^1}$ acts as a tridentate ligand towards

TABLE 1 Crystallographic data of complexes **1–3**

Compound	1	2	3
Empirical formula	$C_{84}H_{106}N_8O_{20}Zn_6$	C_{60} $H_{70}N_4O_2Cu$	$C_{42}H_{48}N_2O_4Cu$
Formula weight	1939.99	942.74	708.36
Temperature/K	293(2)	100(2)	100(2)
Wavelength	0.71073 Å	0.71073 Å	0.71073 Å
Crystal system	Triclinic	Monoclinic	Monoclinic
Space group	*P*-1	*C*2/*c*	$P2_1/n$
a/Å	11.4722(5)	19.3116(13)	13.6798(5)
b/Å	15.0649(10)	11.3985(13)	10.3619(4)
c/Å	15.1378 (8)	25.440(2)	13.8376(5)
α (°)	62.435(6)	90	90
β (°)	89.314(4)	104.418(8)	107.312(2)
γ (°)	84.493(4)	90	90
V/Å^3	2307.0(2)	5423.5(9)	1872.60(12)
Z	1	4	2
ρ_{calc} (g cm^{-3})	1.396	1.155	1.256
Absorption coefficient (mm^{-1})	1.604	0.447	0.626
F(000)	1006	2012	750
Index ranges	$-14 \le h \le 15$ $-12 \le k \le 19$ $-18 \le l \le 19$	$-24 \le h \le 24$ $-14 \le k \le 14$ $-31 \le l \le 28$	$-13 \le h \le 19$ $-14 \le k \le 14$ $-19 \le l \le 19$
Reflections collected	12908	23463	25393
Independent reflections	9911	5562	5712
Goodness-of-fit on F^2	1.054	1.177	1.049
Final *R* indices [$I > 2\sigma(I)$]	$R_1 = 0.0455$ $wR_2 = 0.1047$	$R_1 = 0.0668$ $wR_2 = 0.1464$	$R_1 = 0.0362$ $wR_2 = 0.1053$
R Indices (all data)	$R_1 = 0.0633$ $wR_2 = 0.1178$	$R_1 = 0.1095$ $wR_2 = 0.1667$	$R_1 = 0.0456$ $wR_2 = 0.0993$

Zn(II) ions in which two imine N atoms are anchored with two different zinc atoms rather than with one zinc (for example, Zn(1) is appended to N(9) while Zn(2) is bonded to N(7)). This type of coordination is most stable from the thermodynamic point of view. In case of square pyramidal geometry, Zn(1) and Zn(2) are connected through an oxo bridge and other three coordination positions are occupied by ligand and acetate unit. The fifth coordination position of Zn(1) is anchored by an oxygen atom of a bridging acetate moiety. However, the fifth coordination position of Zn(2) is fulfilled by a terminal acetate group. On the other hand, most interestingly, Zn(3) is attached to O atoms of acetate units to complete its four coordinations to achieve the tetrahedron geometry. In **1**, the phenyl rings containing 2,4,6-trimethyls are almost perpendicular to the phenyl ring having the oxygen atom. All the methyl units from acetate moieties are *trans* to each other.

The single crystal analysis of complex **2** shows that the brown colored crystals crystallizes in monoclinic system with an achiral *C2/c* space group. Unlike complex **1**, complex **2** has a mononuclear structure (Figure 2). The Cu(II) ion presents at the inversion center and is coordinated with the surrounding two oxygen and two nitrogen atoms of $\mathbf{L^1}$ units having the distorted square planar geometry. In this case, the ligand acts as a bidentate chelator rather than tridentate. Actually, amongst two imine nitrogen atoms, one is bonded to the metal ion and other remains free. The coordination with both nitrogen atoms presumably is not thermodynamically stable. The molecules are arranged in AB-AB type of stacking and are formed by two units of $\mathbf{HL^1}$ ligands anchoring Cu(II) ions in the opposite direction to reduce the steric hindrance. Furthermore, complex **2** gets extra stability from the intra C–H .... π interaction between C(21)H(21) and benzene ring of trimethyl aniline unit (as well as C(19)

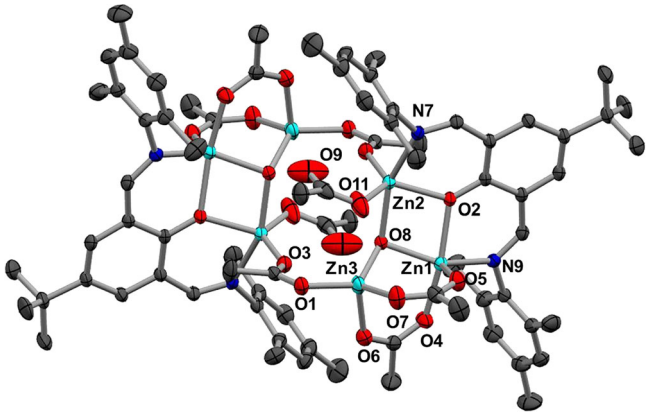

FIGURE 1 The molecular structure of complex **1**; thermal ellipsoids were drawn with 30% probability level; the hydrogen atoms and solvent molecules have been omitted for clarity; Selected bond lengths () and bond angles (°): Zn(1)–O(2) 2.113(2), Zn(1)–N(9) 2.051(3), Zn(1)–O(8) 2.020(2), Zn(2)–O(2) 2.074(2), Zn(2)–N(7) 2.152(3), Zn(2)–O(11) 2.054(4), Zn(3)–O(1) 1.958(2), Zn(3)–O(6) 1.997(3), Zn(3)–O(7) 1.982(3); N(9)–Zn(1)–O(2) 86.94(9), O(4)–Zn(1)–O(2) 93.51(11), N(7)–Zn(2)–O(2) 84.78(9), N(7)–Zn(2)–O(3) 102.72(11), O(1)–Zn(3)–O(6) 105.71(4), O(1)–Zn(3)–O(7) 107.61(11)

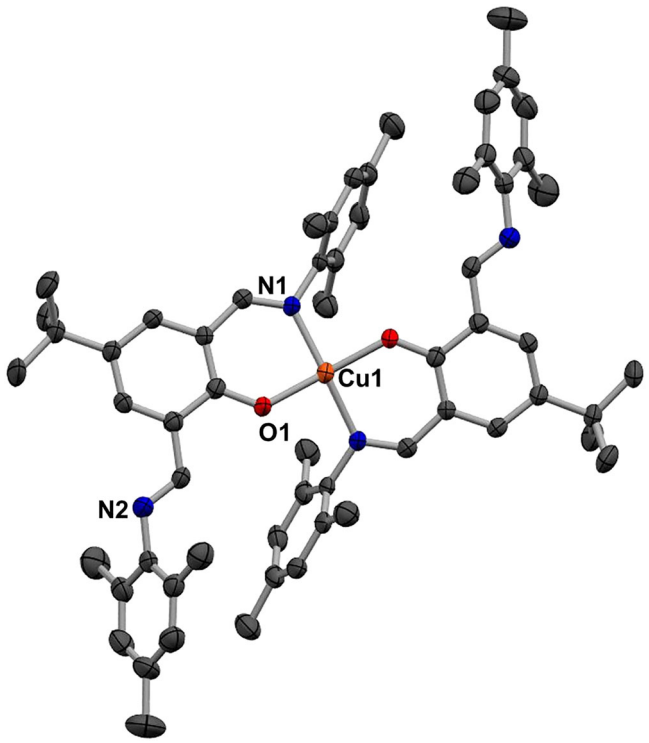

FIGURE 2 The molecular structure of complex **2**; thermal ellipsoids were drawn with 30% probability level and the asymmetric units were labeled; Selected bond lengths () and bond angles (°): Cu(1)–O(1) 1.905(2), Cu(1)–N(1) 1.974(3), Cu(1)–$O(1)^i$ 1.905(2), Cu(1)–$N(1)^i$ 1.974(3); O(1)–Cu(1)–$O(1)^i$ 165.19(16), O(1)–Cu(1)–N(1) 93.05(11), $O(1)^i$–Cu(1)–$N(1)^i$ 93.05(11), $O(1)^i$–Cu(1)–N(1) 88.93(11), O(1)–Cu(1)–$N(1)^i$ 88.93(11)

H(19c) and benzene ring of trimethyl aniline) (Figure S22a†). The C–H .... π interaction ranges from 2.678–2.790 Å as marked with red color and shown in Figure S22b†. The stability of these molecules is further enhanced by the inter C-H .... π interaction with a distance of 2.588 Å which are shown with green dotted lines (Figure S22b†).

On the other hand, the centrosymmetric complex **3** crystallizes in monoclinic system with $P2_1/n$ space group. From Figure 3 it is clear that complex **3** has also a mononuclear structure having one Cu (II) ion with two $\mathbf{L^2}$ ligand skeletons and has slightly distorted square planar geometry. In terms of structural coordination, **3** is quite resemble with **2**. The unsymmetrical ligand acts as a true bidentate unit since it lacks in other imine N atom. The carbonyl oxygen atoms and two *tert*-butyl groups in the phenyl rings are oriented in the opposite direction. Two *tert*-butyl groups along with 2,4,6-trimethyl imino units reside out of the molecular plane. All the bond lengths are in the expected limits. Like the complex **2**, complex **3** is also stabilized by the intramolecular C–H .... π interaction between C(7)H(7) and benzene ring of trimethyl aniline with a distance of 2.656 Å (marked with black dotted lines in Figure S23†). In addition, the molecule is further strengthened by the π–π stacking interaction with a distance of 4.751 Å (displayed in yellow dotted lines in Figure S23†).

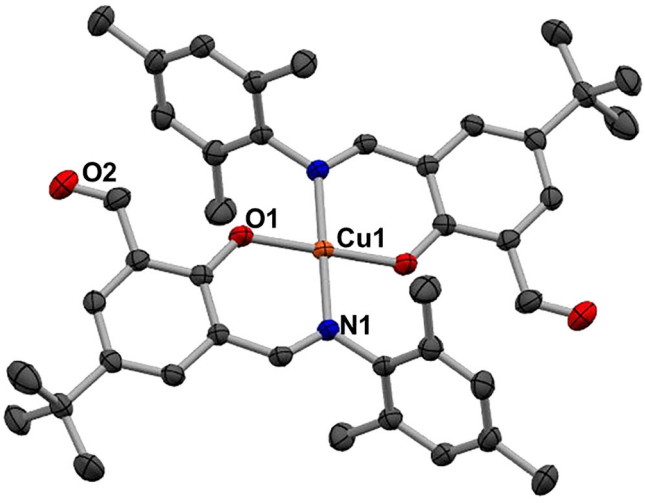

FIGURE 3 The molecular structure of complex **3**; thermal ellipsoids were drawn with 30% probability level and the asymmetric units were labeled; Selected bond lengths () and bond angles (°): Cu(1)–$O(1)^i$ 1.891(10), Cu(1)–O(1) 1.891(10), Cu(1)–$N(1)^i$ 1.998(11), Cu(1)–N(1) 1.998(11); O(1)–Cu(1)–$O(1)^i$ 180.00(6), $O(1)^i$–Cu(1)–$N(1)^i$ 92.47(4), N(1)–Cu(1)–$N(1)^i$ 180.00(6), O(1)–Cu(1)–$N(1)^i$ 87.53(4), $O(1)^i$–Cu(1)–N(1) 87.53(4), O(1)–Cu(1)–N(1) 92.47(4)

3.3 | DNA binding ability

Electron absorption spectroscopy is a widespread and common protocol in order to explore the binding interactions between metal complex and DNA. The absorption spectra for **1** in Tris–HCl/NaCl buffer is depicted in Figure 4 while the absorption spectra for **2** and **3** are shown in Figure S9–S10†. The absorption bands of these complexes (**1**–**3**) in the range of 406–425 nm in the UV spectra are assigned to the intraligand $\pi \rightarrow \pi^*$ transition. With a constant concentration of the concerned complexes (50 μM) and increasing amounts of CT-DNA concentration (0–50 μM), considerable hyperchromisms are observed with a slight red shift. This observation attributes that all the complexes interact significantly with DNA presumably through non-intercalative binding mode *via* accessing multiple hydrogen bonding sites present within both major and minor grooves[60–63] and the electrostatic interaction between positively charged metal ion and the negatively charged DNA phosphate skeleton.[64,65] The classical intercalation may be ruled out due to the bulky structure of **1** (non-planer as well) and the significant non-planarity issues (the phenyl rings containing 2,4,6-trimethyl groups in **2** & **3** are out of the plane completely) in case of **2** & **3**.

The intrinsic binding constants (K_b) of the complexes are calculated using the equation 1 (see experimental part).[9] The binding affinity of the complexes towards CT-DNA decreases in the order **1** ($K_b = 4.82 \times 10^4$ M^{-1}) > **2** ($K_b = 1.81 \times 10^4$ M^{-1}) > **3** ($K_b = 1.32 \times 10^4$ M^{-1}). Nonetheless, these values do imply that the binding capabilities to the CT-DNA are moderate and comparable with the literature precedents.[9,63,65]

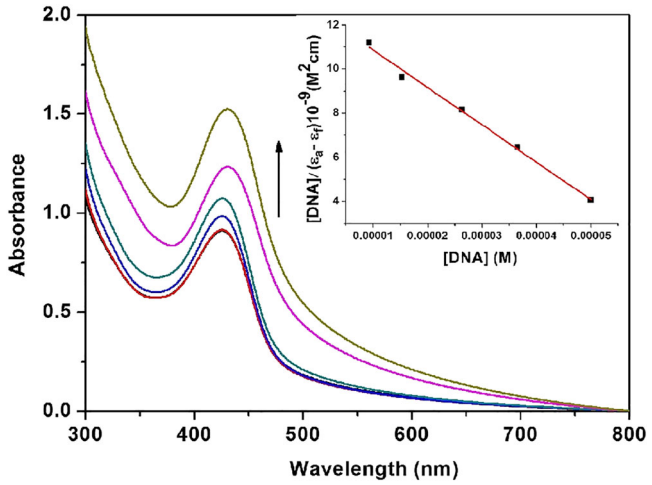

FIGURE 4 Absorption spectra of complex **1** (50 μM) with increasing concentration of CT-DNA (0–50 μM) at room temperature in Tris–HCl/NaCl buffer (pH = 7.2). Inset: Plot of $[DNA]/(\varepsilon_a - \varepsilon_f)$ vs. [DNA] for the absorption titration of CT-DNA with **1**

3.3.1 | Fluorescence titration

To scrutinize further the interacting mode of the aforementioned complexes with DNA, fluorescence quenching experiments were performed using ethidium bromide (EB). The fluorescence intensity of EB is very strong in the presence of DNA owing to the intercalation of EB into the adjacent base pairs of DNA double helix.[66] However, EB emits quite weak fluorescence in its free form. After the addition of a complex, the intercalation between DNA and the complex causes fluorescence quenching by knocking out EB.[67] Nevertheless, the electrostatic interaction may lead to a contraction of the double stranded DNA through neutralizing the negative charges of corresponding phosphate moieties present in the DNA backbone. Consequently, it pushes EB out of the DNA and governs the quenching of the said fluorescence.[68] With the increasing concentration of complexes **1**–**3** (0–50 μM), the fluorescence intensity of EB-DNA system was reduced at a considerable rate (Figure 5 for **1** and Figure S11 − S12† for **2** & **3**). It illustrates that **1**–**3** could bind to CT-DNA *via* the substitution of EB in the EB-DNA mixture.

The apparent binding constants (K_{app}) of **1**–**3** were calculated utilizing the equation 2.[69]

$$K_{EB}[EB] = K_{app}[complex] \quad (2)$$

Where the complex concentration was the value at 50% reduction of the fluorescence intensity of EB and $K_{EB} = 1.0 \times 10^7$ M^{-1}, ([EB] = 9.75×10^{-5} M). The apparent binding constants for **1**–**3** do follow the order **1** ($K_{app} = 4.4 \times 10^5$ M^{-1}) > **2** ($K_{app} = 3.9 \times 10^5$ M^{-1}) > **3** ($K_{app} = 3.2 \times 10^5$ M^{-1}) which are in good agreement with

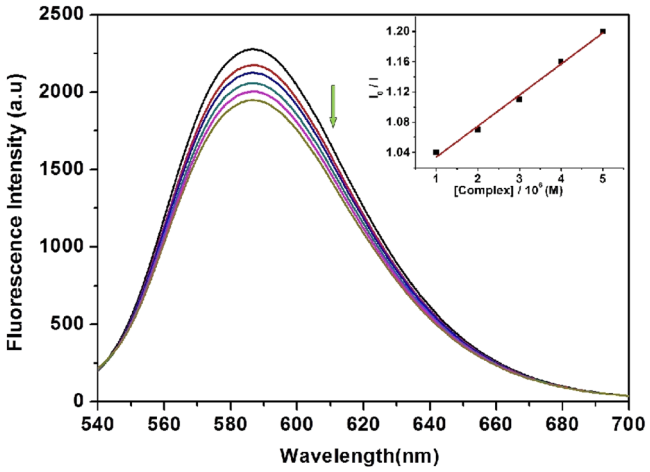

FIGURE 5 Fluorescence quenching spectra of EB bound to CT-DNA by **1** ([complex] = 0–50 μM, λ_{ex} = 510 nm). The arrow indicates the change in intensity upon increasing the complex concentration. Inset: Plot of I_0/I *vs.* [complex]

the results found in electronic absorption titration experiments. In addition, the kinetic parameters for DNA binding are very much comparable with the reported Zn(II) and Cu(II) complexes (Table 2).

3.4 | Protein binding studies

Serum albumins do play a crucial role in the transporting of amino acids, steroids, fatty acids, drugs and metal ions. Due to structural resemblance with human serum albumin, bovine serum albumin (BSA) is one of the most important serum albumin and examined comprehensively. The intrinsic fluorescence of BSA is a predominantly outcome of tryptophan residues mainly Trp-134 and Trp-212. Now, fluorescence spectroscopy is an essential tool for examining the interacting power of metal complexes to BSA. The effect of absence and presence of complex **1** on the fluorescence intensity of BSA is presented in Figure 6 (similar types of spectra for **2** & **3** are illustrated in Figure S13 – S14†).

The noteworthy reduction of intensity of the broad emission spectrum upon the addition of the complex (0–50 μM) to a constant concentration of BSA (10 μM) actually points out the interaction of BSA with the complex. Perhaps this interaction arises owing to the alteration in the tryptophan residues environment. The quenching of fluorescence may be ascribed using Stern-Volmer equation.[69]

$$F_0/F = 1 + K_{SV}[Q] = 1 + K_q\tau_0[Q] \quad (3)$$

Where F_0 and F correspond to the fluorescence intensities in the absence and presence of the concerned quencher, K_q is the quenching rate constant, τ_0 represents the average lifetime of the biomolecule without the quencher (~10^{-8} s),[70] K_{SV} is the Stern-Volmer quenching constant and [Q] is the concentration of the quencher. K_{SV} can be found out from the slope of the plot of F_0/F *vs.* [Q]. The obtained values of K_{SV} and K_q of complexes **1**–**3** are summarized in Table 3.

It is very clear from these values that all the complexes are the potential quenchers of BSA in terms of binding

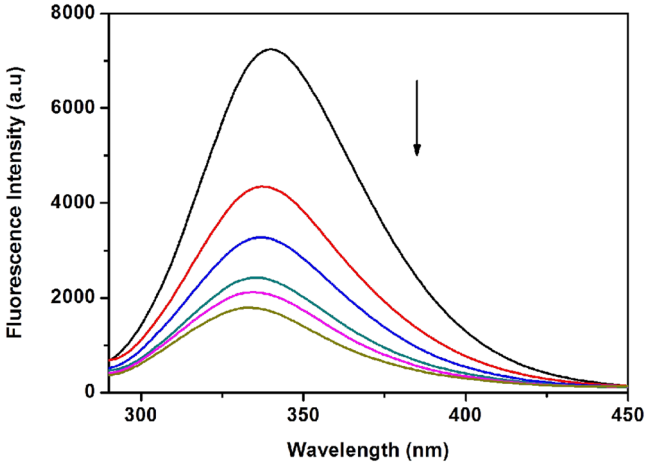

FIGURE 6 Fluorescence spectra of BSA with gradual increment of concentration of complex **1** at room temperature. [BSA] = 10 μM, and [complex **1**] = 0–50 μM

prospects. Amongst three complexes, **1** exhibits much higher binding capabilities towards BSA in comparison with **2** or **3**. However, the K_q values (> 10^{12} M^{-1} s^{-1}) are greater in comparison to variously diversified quenchers for biopolymers fluorescence (2×10^{10} M^{-1} s^{-1}). It signifies that the static quenching pathway is favoured rather than the dynamic one.[70] Again, the UV–visible spectra of BSA were recorded further prior to and after the addition of the complexes to investigate the structural change related to the peptide strands in BSA (Figure 7 and Figure S15 – S16†). The intensity of the absorption maxima is substantially enhanced on employing of complexes (10 μM) with slight red shift (2–3 nm). This observation again manifests the formation of a ground state complex associated with BSA and the aforesaid compounds.[71,72]

In case of the static mode of quenching, the binding constant (K_b) and the number of binding sites (n) per albumin can be ascertained utilizing the Scatchard equation.[73]

$$\log(I_0–I)/I = \log K_b + n \log[Q] \quad (4)$$

The K_b and n values are calculated from the intercept and slope of the double logarithmic curve of $\log(I_0 - I)/I$ *vs.*

TABLE 2 Comparison of kinetic parameters for **1**–**3** with reported Zn(II) and Cu(II) complexes

Complex	K_b (M^{-1})	K_{app} (M^{-1})	Ref.
1	4.82×10^4	4.4×10^5	This Work
2	1.81×10^4	3.9×10^5	This Work
3	1.32×10^4	3.2×10^5	This Work
$[Zn\ (Hqasesc)_2]^{2+}$	8.92×10^4	Not Determined	[92]
$[Zn_2(L)]\cdot(ClO_4)_2$	1.16×10^4	1.1×10^5	[93]
$[Cu(H_2L_1)Cl]\cdot CH_3OH$	2.28×10^3	Not Determined	[94]
$Cu_4(HL_2)_2(H_2L_2)_2(H_2O)(C_2H_5OH)]\cdot 2(ClO_4)\cdot 2(C_2H_5OH)$	1.35×10^4	Not Determined	[94]

TABLE 3 BSA binding constants of complexes **1–3** and comparison with reported Zn(II) and Cu(II) complexes

Complex	K_{sv} (M^{-1})	K_q (M^{-1})	K_b (M^{-1})	n	Ref
1	5.95×10^4	9.59×10^{12}	2.9×10^4	0.93	This work
2	2.99×10^4	4.84×10^{12}	3.4×10^3	0.76	This work
3	2.4×10^4	3.87×10^{12}	3.1×10^3	0.52	This work
$[Zn\ (Hqasesc)_2]^{2+}$	2.01×10^6	2.82×10^{14}	Not Determined	0.89	[92]
$Zn_2(L_1)_2Cl_2](ClO_4)_2{\cdot}C_2H_5OH$	9.97×10^4	9.97×10^{12}	1.19×10^2	0.48	[95]
$[Cu(H_2L_1)Cl]{\cdot}CH_3OH$	0.47×10^5	Not Determined	9.16×10^3	1.03	[94]
$Cu_4(HL_2)_2(H_2L_2)_2(H_2O)(C_2H_5OH)]{\cdot}2(ClO_4){\cdot}2(C_2H_5OH)$	1.36×10^5	Not Determined	6.91×10^5	0.87	[94]

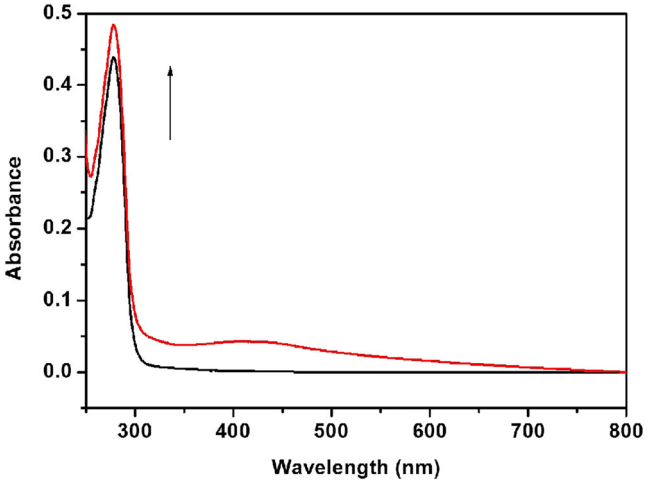

FIGURE 7 UV–Visible spectra of BSA in the absence complex **1** (Black line). The absorption of BSA in the presence of complex **1** (Red line). [BSA] = [complex **1**] = 10 μM

log[Q] (Table 3). Table 3 demonstrates that the hexanuclear Zn (II) complex (**1**) has a quite higher K_b value for BSA than the two mononuclear Cu (II) complexes (**2** and **3**). Based on the K_b values, it points out that the nuclearity may display a significant role in the protein binding experiment since the ligand moiety is almost the same. In addition, the *n* values are near about one which reveals the involvement of a single binding site in BSA for the concerned complexes.

3.5 | Catecholase activity

Catechol oxidase which is a candidate of the type-III copper proteins uses dioxygen molecule as an oxidant.[74] This particular enzyme corresponding to the group of polyphenol oxidases catalyzes the oxidation of several *o*-diphenols to their respective *o*-quinones.[75–77] Quinones are quite reactive molecules which can trigger auto polymerization to generate a brown pigment namely melanin. Perhaps this process is accountable to prevent the tissues from the damage against pathogen and insects in higher plants.[78]

Since dicopper(II) units are the centers of activity in catechol oxidase, the preferred choice to several research groups is dinuclear Cu(II) systems as catalysts for catechol oxidation reaction.[79–82] In contrast with various dinuclear Cu(II) systems, a few mononuclear Cu(II) complexes[83–86] and Zn(II) based compounds bearing diversified ligands with N/O donors were reported in the literature.[6,51,87–89] Thus, there is an excellent scope of exploitation of such mononuclear Cu (II) units and hexanuclear Zn (II) compound as catalysts towards the conversion of 3,5-di-*tert*-butylcatechol (3,5-DTBC) to 3,5-di-*tert*-butylquinone (3,5-DTBQ).

In order to determine the catecholase activity of **1–3**, 3,5-DTBC was utilized as a model substrate. 3,5-DTBC is mainly used due to its low reduction potential (easy oxidation to quinone) and the presence of the bulky *tert*-butyl units preventing further oxidation like ring opening. However, 3,5-DTBQ is enormously stable and has a characteristic absorption peak at around 400 nm in acetonitrile (λ_{max}~402 nm in methanol). The catalytic activity of complexes **1–3** towards the oxidation of 3,5-DTBC to 3,5-DTBQ was investigated in acetonitrile (in case of **1**) and methanol (in case of **2** and **3**). In this regard, 1×10^{-4} M solutions of **1–3** were mixed with 1×10^{-2} M (100 equivalents) of 3,5-DTBC under aerobic condition at ambient temperature. The advancement of the reaction was monitored by UV–vis spectroscopy as shown in the Figure 8 (for **1**) and Figure S17 − S18† (for **2** and **3**) after each 8 minutes intervals. Upon the addition of the substrate, the appearance of a new band ~ 400 nm was observed owing to the formation of 3,5-DTBQ. The concentration of the oxidized product was increased with time leading to the bigger and taller absorption bands. All the said complexes do behave in a similar fashion and demonstrate a very smooth conversion of 3,5-DTBC to 3,5-DTBQ. Hence, it proves the efficacy of these complexes as catalysts for the oxidation of 3,5-DTBC. Besides this, the formation of the oxidized products was further

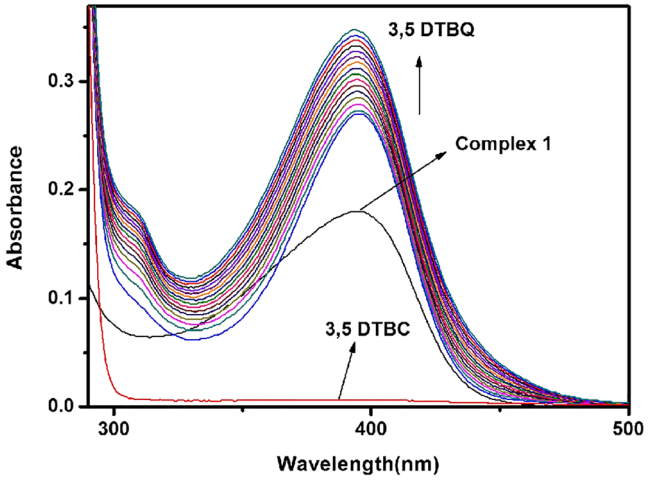

FIGURE 8 UV–vis spectra illustrating the growth of quinone band at ~ 400 nm after the addition of 100-fold 3,5-DTBC to a solution containing complex **1**

confirmed by gas chromatography techniques (Figure S27–S29).

The kinetic prospects of this oxidation reaction using **1**–**3** were ascertained through the initial rate method by analyzing the increment of the quinone band with time. In this regard, at low concentrations of 3,5-DTBC, the rate has first order dependence for all three complexes. However, saturation kinetics are observed at higher concentrations of 3,5-DTBC. Based on the famous Michaelis–Menten equation of enzyme kinetics, the maximum velocity (V_{max}), binding constant (K_M) and turnover number (k_{cat}) were found out from Lineweaver-Burk plot of 1/[rate] *vs.* 1/[S] (Figure 9 for **1** and Figure S19–20 for **2** & **3**†) using the following equation.

$$\frac{1}{\nu} = \frac{K_M}{V_{max}} \times \frac{1}{[S]} + \frac{1}{V_{max}}$$

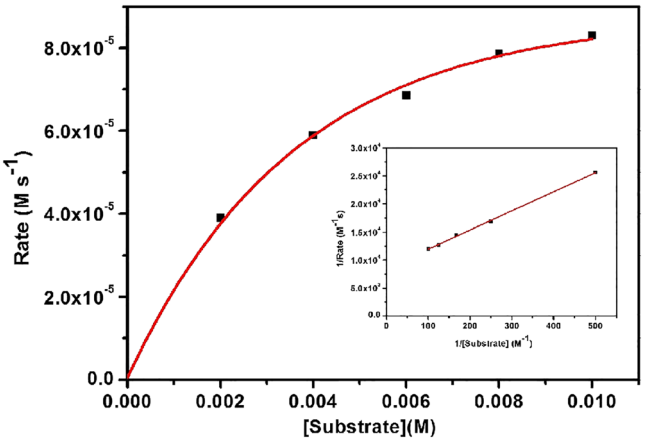

FIGURE 9 Plot of the rate (ν) *vs.* substrate concentration ([S]) for complex **1**. Inset: corresponding Lineweaver–Burk plot of 1/rate against 1/[substrate]

Where ν is the rate of the reaction and [S] is the substrate concentration. The values of aforesaid kinetic parameters for **1**–**3** are depicted in Table 4.

From the Table 4, it is clear that complex **1** displays highest k_{cat} (4.1×10^3 h^{-1}) and V_{max} (1.16×10^{-4} M s^{-1}) values among all three complexes. So, these complexes are active catalysts for this oxidation reaction considering the all the kinetic parameters and the order of the said activity is **1** > **2** > **3**.

Generally, the conversion to quinone from catechol is a two electron oxidation reaction. Now, it is rather crucial to understand the probable cause behind the activity of the complexes for this conversion. Interestingly, either metal based redox participation or a ligand oriented free radical route is accountable for that kind of activity.[90a] To establish the actual cause, we have accomplished EPR spectral studies of **1** (at 77 K), **2** & **3** (at room temp) before and after mixing of 3,5-DTBC with 10^{-3} M acetonitrile solution of concerned complexes in an inert atmosphere. The EPR studies exhibit a sharp signal at $g_{\sim}2$ in case of **1** after mixing the catechol as shown in Figure 10 which confirm the generation of free radical. Although, during the experiment, we have found that **1** is an EPR inactive species (Since Zn^{+2} ion is a d^{10} system). Whereas, the EPR spectra of **2** and **3** represent four hyperfine peaks ($g_{\parallel}$ = 2.137 & $g_{\perp}$ = 2.039 for **2** and $g_{\parallel}$ = 2.137 & $g_{\perp}$ = 2.035 for **3**; $A_{\parallel}$ = 78.1 G for **2** & $A_{\parallel}$ = 78.7 G for **3**) in absence of 3,5-DTBC (see Figure 11 for **2** and Figure S21† for **3**). Now, EPR spectroscopy can differentiate the associated ground states ($d_{x^2-y^2}$ and d_{z^2}) using the g tensor values of the anisotropic spectra. $d_{x^2-y^2}$ will be the ground state when the complex has elongated octahedral, square pyramidal or square planar geometries. Whereas, the ground state will be d_{z^2} for a squeezed octahedral or trigonal bipyramidal geometry around the metal ion.[90b] In this case, the axial EPR spectra along with $g_{\parallel} > g_{\perp} > 2$ order emphasize that both the Cu (II) complexes have square planar geometries with $d_{x^2-y^2}$ orbital as a ground state.[90c–e] Slightly higher g values accentuate the presence of little distortion in the Cu (II) complexes which is also clear from single crystal X-ray diffraction studies.[90c–e] After the addition of 3,5-DTBC to **2** and **3** separately, an additional peak was appeared at g = 2.004 and g = 1.99 for **2** & **3** respectively (Figure 11 and Figure S21†). This indicates the involvement of free radical in the oxidation process. Nevertheless, the EPR signals of Cu (II) ion in **2** and **3** remain unchanged after the addition of 3,5-DTBC which precludes the possibility of metal based redox participation.[7] So, from the EPR signals, we can conclude that the oxidation of 3,5-DTBC to 3,5-DTBQ in the presence of aforementioned complexes goes through a ligand oriented radical pathway.

TABLE 4 Kinetic parameters for the catecholase activity of **1–3** and comparison with reported Zn(II) and Cu(II) complexes

Complex	V_{max} (M s^{-1})	K_m (M)	k_{cat} (h^{-1})	Ref.
1	$(1.16 \pm 0.05) \times 10^{-4}$	$(3.95 \pm 0.04) \times 10^{-3}$	4.1×10^3	This Work
2	$(8.46 \pm 0.09) \times 10^{-5}$	$(5.1 \pm 0.07) \times 10^{-3}$	3.0×10^3	This Work
3	$(4.35 \pm 0.15) \times 10^{-5}$	$(3.6 \pm 0.10) \times 10^{-3}$	1.5×10^3	This Work
$[Zn_3(L)(NCS)_2](NO_3)_2{\cdot}CH_3OH{\cdot}H_2O$	2.58×10^{-5}	1.88×10^{-3}	9.28×10^2	[6]
$[Zn_3(L_1)_2(\mu OAc)_2\ (CH_3OH)_4]$	3.0×10^{-4}	1.06×10^{-3}	1.33×10^3	[51]
[CuL (NCO)]	1.31×10^{-7}	2.27×10^{-3}	23.58	[7]
[Cu (sal-ppzH)Cl_2]	9.85×10^{-3} mmol min^{-1}	5.3×10^{-3}	1.182×10^4	[86]

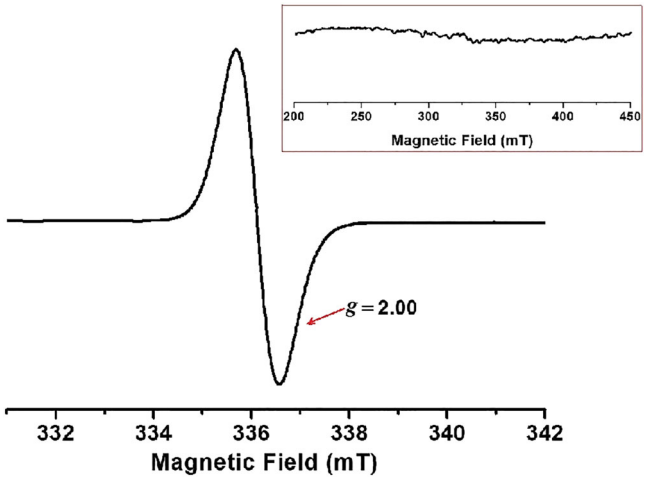

FIGURE 10 EPR spectrum of complex **1** after the addition of 3,5-DTBC. Inset: EPR spectrum of **1** in absence of 3,5-DTBC

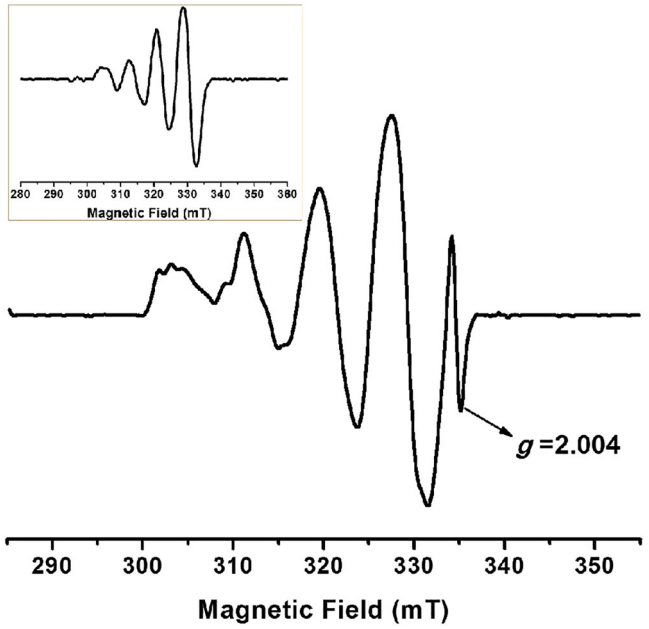

FIGURE 11 EPR spectrum of complex **2** after the addition of 3,5-DTBC. Inset: EPR spectrum of **2** in the absence of 3,5-DTBC

3.6 | Anticancer activity

The optimistic outcomes which are acquired from DNA binding, protein binding and catecholase activity evaluations of complexes **1–3**, motivated us further to investigate the cytotoxicity study of the complexes against HeLa cells (human cervical cancer cell lines).

MTT assay has been utilized to assess *in vitro* cytotoxicity of the said complexes. The metabolic action in cells was scrutinized by their capabilities to reduce the tetrazo-

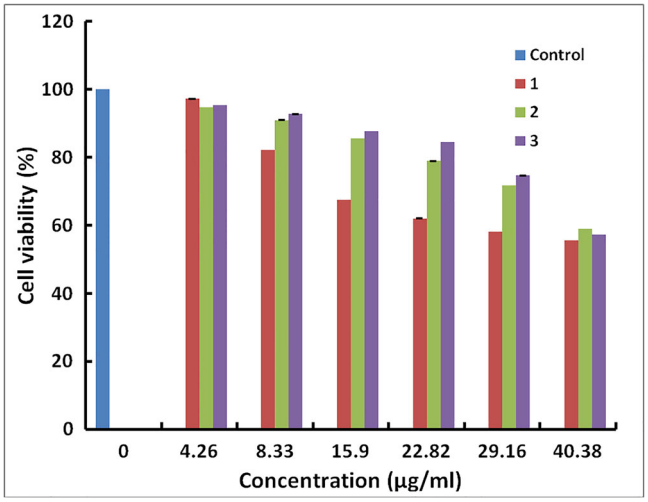

FIGURE 12 The extent of cell viability of HeLa cells after the treatment with complexes **1–3** for 48 hr

TABLE 5 Summary of IC_{50} values of **1–3** against HeLa cell lines

Compound	IC_{50} value (µM)
1	25.3
2	53
3	66.5
Cisplatin	15[a]

[a]See reference 96,97.

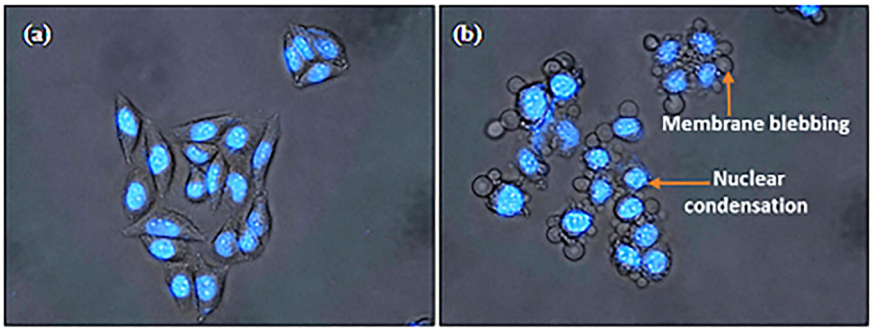

FIGURE 13 Inverted microscopic images after staining the nucleus using Hoechst 33342. (a) control cells show intact cellular morphology with evenly stained nucleus and (b) complex **1** treated cells depict membrane blebbing and condensed nucleus with intensely staining

lium ring of yellowish MTT to dark blue formazan. This reduction process is actually based on the fact that the mitochondrial enzyme succinate dehydrogenase in living cells (instead of dead cells) is responsible for the cleaving of the tetrazolium ring. The cytotoxic activity of **1**–**3** against HeLa cells was examined after 48 hr of incubation period. All the compounds are potent inhibitor of cell growth as depicted in Figure 12. Here, cell inhibition is expressed in terms of IC_{50} value and summarized in Table 5. From Table 5, it is quite evident that all the complexes show considerable cytotoxic activity with IC_{50} values in the range of 25.3–66.5 μM. The potential of the aforementioned complexes as anticancer drug decreases in the order **1** > **2** > **3**.

Most interestingly, IC_{50} value of **1** is relatively closer with famous anticancer drug cisplatin in comparison with **2** or **3** despite of having a huge structure (in case of **1**). However, all the complexes are less toxic compared to the cisplatin. The anticancer activity of metal complexes has heavily relied upon DNA binding aspects which lead to destroy its secondary structure. As a consequence, the replication and transcription processes are suppressed due to the prevention of normal functioning of DNA. This triggers the cell death ultimately if the repair work of DNA is not restored. The observations of the *in vitro* cytotoxicity are at par with DNA and protein binding studies which confirm again the interaction between DNA and metal complexes.

In order to investigate the mode of cell death, complex **1** was treated with Hela cells (as the IC_{50} value is close to that of cisplatin) and monitored the morphological changes of the cells with Hoechst 33342 nuclear staining. After 12 hours of treatment, the treated cells (Figure 13b) became circular with prominent membrane protrusion while such cellular features were not observed in the case of the untreated cells (Figure 13 a). As the formation of the small blister and nuclear condensation are the hallmark indicators of apoptotic cells,[91] the study confirmed that **1** has the potential anticancer activity to cause cell death via an apoptotic pathway.

4 | CONCLUSIONS

A novel hexanuclear Zn(II) and two mononuclear Cu(II) complexes containing imino phenolate ligand unit are prepared and structurally characterized. Subsequently, the potential of these compounds towards DNA binding, protein binding, catecholase and cytotoxic activities have been thoroughly investigated. It is observed that all the complexes interact to CT-DNA *via* non-intercalative binding approach which has been monitored by spectroscopic techniques. Also, they show excellent ability to bind protein which is an essential requirement for exhibiting anticancer activity. The pathway of quenching of BSA was originated from the static mode instead of the dynamic one. On the other hand, they are efficient catalysts for the oxidation of 3,5-DTBC to 3,5-DTBQ under aerobic condition. Besides, all the complexes have portrayed noteworthy *in vitro* cytotoxic activity towards the HeLa cell lines and the IC_{50} value was found to be a little bit higher in case of zinc complex compared to other two copper compounds. Hoechst 33342 nuclear staining studies demonstrate that the apoptotic mechanism is the prime reason of the cell death.

ACKNOWLEDGMENTS

TKS thanks to SERB, Govt. of India for financial support (File no. ECR/2016/000681) and acknowledges NIT Durgapur for providing the infrastructure. SSM thanks to NIT Durgapur for giving the fellowship.

CCDC 1852303 − 1852305 contain the supplementary crystallographic data for this paper. The data can be obtained free of charge *via* www.ccdc.cam.ac.uk/structures.

CONFLICT OF INTEREST

There are no conflicts to declare.

ORCID

Tanmoy Kumar Saha https://orcid.org/0000-0002-5606-4973

REFERENCES

[1] K. Zheng, L. Jiang, Y.-T. Li, Z.-Y. Wu, C.-W. Yan, *RSC Adv.* **2015**, *5*, 51730.

[2] C. Balakrishnan, S. Natarajan, M. A. Neelakantan, *RSC Adv.* **2016**, *6*, 102482.

[3] D. S. Raja, N. S. P. Bhuvanesh, K. Natarajan, *Dalton Trans.* **2012**, *41*, 4365.

[4] T. S. Basu Baul, S. Kundu, A. Linden, N. Raviprakash, S. K. Manna, M. F. C. Guedes da Silva, *Dalton Trans.* **2014**, *43*, 1191.

[5] S. A. Hosseini-Yazdi, A. Mirzaahmadi, A. A. Khandar, V. Eigner, M. Dušek, M. Mahdavi, S. Soltani, F. Lotfipour, J. White, *Polyhedron* **2017**, *124*, 156.

[6] S. Pal, B. Chowdhury, M. Patra, M. Maji, B. Biswas, *Spectrochim. Acta - Part A Mol. Biomol. Spectrosc.* **2015**, *144*, 148.

[7] M. Shyamal, T. K. Mandal, A. Panja, A. Saha, *RSC Adv.* **2014**, *4*, 53520.

[8] M. A. Malik, O. A. Dar, P. Gull, M. Y. Wani, A. A. Hashmi, *Med. Chem. Commun.* **2018**, *9*, 409.

[9] W.-J. Lian, X.-T. Wang, C.-Z. Xie, H. Tian, X.-Q. Song, H.-T. Pan, X. Qiao, J.-Y. Xu, *Dalton Trans.* **2016**, *45*, 9073.

[10] D. Mahendiran, R. S. Kumar, V. Viswanathan, D. Velmurugan, A. K. Rahiman, *Dalton Trans.* **2016**, *45*, 7794.

[11] P. Gurumoorthy, D. Mahendiran, D. Prabhu, C. Arulvasu, A. K. Rahiman, *RSC Adv.* **2014**, *4*, 42855.

[12] T. W. Hambley, *Dalton Trans.* **2007**, 4929.

[13] F. Arnesano, G. Natile, *Coord. Chem. Rev.* **2009**, *253*, 2070.

[14] B. Rosenberg, L. Van Camp, T. Krigas, *Nature* **1965**, *205*, 698.

[15] Y. W. Jung, S. J. Lippard, *Chem. Rev.* **2007**, *107*, 1387.

[16] M. Galanski, M. A. Jakupec, B. K. Keppler, *Curr. Med. Chem.* **2005**, *12*, 2075.

[17] I. Ott, R. Gust, *Pharm. Unserer. Zeit.* **2006**, *35*, 124.

[18] I. Ali, W. A. Wani, K. Saleem, A. Haque, *Anticancer Agents Med Chem.* **2013**, *13*, 296.

[19] W. A. Wani, U. Baig, S. Shreaz, R. A. Shiekh, P. F. Iqbal, E. Jameel, A. Ahmad, S. H. Mohd-Setapar, M. Mushtaque, L. Ting Hun, *New J. Chem.* **2016**, *40*, 1063.

[20] C. Rajarajeswari, R. Loganathan, M. Palaniandavar, E. Suresh, A. Riyasdeen, M. A. Akbarsha, *Dalton Trans.* **2013**, *42*, 8347.

[21] M. Mohanraj, G. Ayyannan, G. Raja, C. Jayabalakrishnan, *Appl. Organomet. Chem.* **2017**, *31*, e3582.

[22] D. Krajčiová, M. Melník, E. Havránek, A. Forgácsová, P. Mikuš, *J. Coord. Chem.* **2014**, *67*, 1493.

[23] K. Mancha Madha, P. Gurumoorthy, S. Arul Antony, N. Ramalakshmi, *J. Mol. Struct.* **2017**, *1143*, 478.

[24] C. H. Ng, S. M. Kong, Y. L. Tiong, M. J. Maah, N. Sukram, M. Ahmad, A. S. B. Khoo, *Metallomics* **2014**, *6*, 892.

[25] J. G. Deng, Y. Gou, W. Chen, X. Fu, H. Deng, *Bioorg. Med. Chem.* **2016**, *24*, 2190.

[26] Y. Sikdar, R. Modak, D. Bose, S. Banerjee, D. Bieńko, W. Zierkiewicz, A. Bieńko, K. D. Saha, S. Goswami, *Dalton Trans.* **2015**, *44*, 8876.

[27] a) M. F. Zaltariov, M. Hammerstad, H. J. Arabshahi, K. Jovanović, K. W. Richter, M. Cazacu, S. Shova, M. Balan, N. H. Andersen, S. Radulović, J. Reynisson, K. K. Andersson, V. B. Arion, *Inorg. Chem.* **2017**, *56*, 3532. b) C. Santini, M. Pellei, V. Gandin, M. Porchia, F. Tisato, C. Marzano, *Chem. Rev.* **2014**, *114*, 815.

[28] Y.-P. Zhang, Z.-Y. Ma, C.-Y. Gao, X. Qiao, J.-L. Tian, W. Gu, X. Liu, J.-Y. Xu, J.-Z. Zhao, S.-P. Yan, *New J. Chem.* **2016**, *40*, 7513.

[29] B. S. Mendiguchia, I. Aiello, A. Crispini, *Dalton Trans.* **2015**, *44*, 9321.

[30] Q. Huang, Z. Pan, P. Wang, Z. Chen, X. Zhang, H. Xu, *Bioorg. Med. Chem. Lett.* **2006**, *16*, 3030.

[31] S. Emami, S. J. Hosseinimehr, S. M. Taghdisi, S. Akhlaghpoor, *Bioorg. Med. Chem. Lett.* **2007**, *17*, 45.

[32] M. T. Kaczmarek, R. Jastrza, E. Hołderna-Kedzia, W. Radecka-Paryzek, *Inorg. Chim. Acta* **2009**, *362*, 3127.

[33] H. Sakurai, Y. Yoshikawa, H. Yasui, *Chem. Soc. Rev.* **2008**, *37*, 2383.

[34] Z. H. Chohan, M. Arif, M. Sarfraz, *Appl. Organomet. Chem.* **2007**, *21*, 294.

[35] V. P. Singh, A. Katiyar, *J. Coord. Chem.* **2008**, *61*, 3200.

[36] A. Nakayama, M. Hiromura, Y. Adachi, H. Sakurai, *J. Biol. Inorg. Chem.* **2008**, *13*, 675.

[37] J. A. Drewry, P. T. Gunning, *Coord. Chem. Rev.* **2011**, *255*, 459.

[38] Y. Yoshikawa, H. Yasui, *Curr. Top. Med. Chem.* **2012**, *12*, 210.

[39] S. Anbu, S. Kamalraj, B. Varghese, J. Muthumary, M. Kandaswamy, *Inorg. Chem.* **2012**, *51*, 5580.

[40] D. Pucci, T. Bellini, A. Crispini, I. D'Agnano, P. F. Liguori, P. Garcia-Orduna, S. Pirillo, A. AValentini, G. Zanchetta, *Med. Chem. Commun.* **2012**, *3*, 462.

[41] Y. Nakamura, Y. Taruno, M. Sugimoto, Y. Kitamura, H. L. Seng, S. M. Kong, C. H. Ng, M. Chikira, *Dalton Trans.* **2013**, *42*, 3337.

[42] P. U. Maheswari, S. Barends, S. O. Yaman, P. Hoog, H. Casellas, S. J. Teat, C. Massera, M. Lutz, A. L. Spek, G. P. vanWezel, P. Gamez, J. Reedijk, *Chem. Eur. J.* **2007**, *13*, 5213.

[43] C. Bazzicalupi, A. Bencini, A. Bianchi, T. Biver, A. Boggioni, S. Bonacchi, A. Danesi, C. Giorgi, P. Gratteri, A. M. Ingraín, F. Secco, C. Sissi, B. Valtancoli, M. Venturini, *Chem. A Eur. J.* **2008**, *14*, 184.

[44] P. F. Liguori, A. Valentini, M. Palma, A. Bellusci, S. Bernardini, M. Ghedini, M. L. Panno, C. Pettinari, F. Marchetti, A. Crispini, D. Pucci, *Dalton Trans.* **2010**, *39*, 4205.

[45] G.−. C. Kuang, J. R. Allen, M. A. Baird, B. T. Nguyen, L. Zhang, T. J. Morgan Jr., C. W. Levenson, M. W. Davidson, L. Zhu, *Inorg. Chem.* **2011**, *50*, 10493.

[46] R. A. Peralta, A. J. Bortoluzzi, B. de Souza, R. Jovito, F. R. Xavier, R. A. A. Couto, A. Casellato, F. Nome, A. Dick, L. R. Gahan, G. Schenk, G. R. Hanson, F. C. S. de Paula, E. C. P.

Maia, S. P. Machado, P. C. Severino, C. Pich, T. Bortolotto, H. Terenzi, E. E. Castellano, A. Neves, M. J. Riley, *Inorg. Chem.* **2010**, *49*, 11421.

[47] C.-H. Leung, S. Lin, H.-J. Zhong, D.-L. Ma, *Chem. Sci.* **2015**, *6*, 871.

[48] A. K. Renfrew, *Metallomics* **2014**, *6*, 1324.

[49] S. Budagumpi, N. V. Kulkarni, G. S. Kurdekar, M. P. Sathisha, V. K. Revankar, *Eur. J. Med. Chem.* **2010**, *45*, 455.

[50] S. Tabassum, S. Amir, F. Arjmand, C. Pettinari, F. Marchetti, N. Masciocchi, G. Lupidi, R. Pettinari, *Eur. J. Med. Chem.* **2013**, *60*, 216.

[51] D. Dey, G. Kaur, A. Ranjani, L. Gayathri, P. Chakraborty, J. Adhikary, J. Pasan, D. Dhanasekaran, A. R. Choudhury, M. A. Akbarsha, N. Kole, B. Biswas, *Eur. J. Inorg. Chem.* **2014**, *2014*, 3350.

[52] S. Anbu, R. Ravishankaran, A. A. Karande, M. Kandaswamy, *Dalton Trans.* **2012**, *41*, 12970.

[53] L. Wang, W.-H. Sun, L. Han, Z. Li, Y. Hu, C. He, C. Yan, *J. Organomet. Chem.* **2002**, *650*, 59.

[54] G. M. Sheldrick, *University of Göttingen*, Göttingen, Germany **1994**.

[55] W. T. Pennington, *J. Appl. Cryst.* **1999**, *32*, 1028.

[56] L. J. Farrugia, *J. Appl. Cryst.* **1997**, *30*, 565.

[57] O. V. Dolomanov, L. J. Bourhis, R. J. Gildea, J. A. K. Howard, H. Puschmann, *J. Appl. Cryst.* **2009**, *42*, 339.

[58] J. Marmur, *J. Mol. Biol.* **1961**, *3*, 208.

[59] a) R. Reichmann, S. A. Rice, C. A. Thomas, P. Doty, *J. Am. Chem. Soc.* **1954**, *76*, 3047. b) M. Tanaka, K. Ohkubo, S. Fukuzumi, *J. Phys. Chem. A* **2006**, *110*, 11214.

[60] N. Zhang, Y.-H. Fan, C.-F. Bi, Y. Zhao, X. Zhang, D.-M. Zhang, G.-M. Huang, *Transition Met. Chem.* **2013**, *38*, 463.

[61] C. L. Kielkopf, S. White, J. W. Szewczyk, J. M. Turner, E. E. Baird, P. B. Dervan, D. C. Rees, *Science* **1998**, *282*, 111.

[62] C. O. Pabo, R. T. Sauer, *Annu. Rev. Biochem.* **1984**, *53*, 293.

[63] G. Barone, A. Terenzi, A. Lauria, A. M. Almerico, J. M. Leal, N. Busto, B. García, *Coord. Chem. Rev.* **2013**, *257*, 2848.

[64] A. Sigel, H. Sigel, *Metal Ions in Biological Systems*, vol. 32, Marcel Dekker, New York, **1996**.

[65] A. Meenongwa, R. F. Brissos, C. Soikum, P. Chaveerach, P. Gamez, Y. Trongpanich, U. Chaveerach, *New J. Chem.* **2016**, *40*, 5861.

[66] F. J. Meyeralmes, D. Porschke, *Biochemistry* **1993**, *32*, 4246.

[67] R. F. Pasternack, M. Caccam, B. Keogh, T. A. Stephenson, A. P. Williams, E. J. Gibbs, *J. Am. Chem. Soc.* **1991**, *113*, 6835.

[68] M. Yu, L. Liu, S. Wang, *J. Polym. Sci. A Polym. Chem.* **2008**, *46*, 7462.

[69] J. R. Lakowicz, G. Weber, *Biochemistry* **1973**, *12*, 4161.

[70] W. R. Ware, *J. Phys. Chem.* **1962**, *66*, 455.

[71] Y. J. Hu, Y. Ou-Yang, C. M. Dai, Y. Liu, X. H. Xiao, *Biomacromolecules* **2010**, *11*, 106.

[72] D. S. Raja, G. Paramaguru, N. S. P. Bhuvanesh, J. H. Reibenspies, R. Renganathan, K. Natarajan, *Dalton Trans.* **2011**, *40*, 4548.

[73] G. Scatchard, *Chem. Rev.* **1949**, *44*, 7.

[74] T. Klabunde, C. Eicken, J. C. Sacchettini, B. Krebs, *Nat. Struct. Biol.* **1998**, *5*, 1084.

[75] I. A. Koval, P. Gamez, C. Belle, K. Selmeczi, J. Reedijk, *Chem. Soc. Rev.* **2006**, *35*, 814.

[76] R. Than, A. A. Feldmann, B. Krebs, *Coord. Chem. Rev.* **1999**, *182*, 211.

[77] K. Selmeczi, M. Reglier, M. Giorgi, G. Speier, *Coord. Chem. Rev.* **2003**, *245*, 191.

[78] B. J. Deverall, *Nature* **1961**, *189*, 311.

[79] N. A. Rey, A. Neves, A. J. C. T. Bortoluzzi, C. T. Pich, H. Terenzi, *Inorg. Chem.* **2007**, *46*, 348.

[80] C. Belle, C. Beguin, I. Gautier-Luneau, S. Hamman, C. Philouze, J. L. Pierre, F. Thomas, S. Torelli, *Inorg. Chem.* **2002**, *41*, 479.

[81] S. J. Smith, C. J. Noble, R. C. Palmer, G. R. Hanson, G. Schenk, L. R. Gahan, M. Riley, *J. Biol. Inorg. Chem.* **2008**, *13*, 499.

[82] J. Ackermann, F. Meyer, E. Kaifer, H. Pritzkow, *Chem. A Eur. J.* **2002**, *8*, 247.

[83] Z.-F. Chen, Z.-R. Liao, D.-F. Li, W.-K. Li, X.-G. Meng, *J. Inorg. Biochem.* **2004**, *98*, 1315.

[84] Á. Kupán, J. Kaizer, G. Speier, M. Giorgi, M. Réglier, F. Pollreisz, *J. Inorg. Biochem.* **2009**, *103*, 389.

[85] M. K. Panda, M. M. Shaikh, R. J. Butcher, P. Ghosh, *Inorg. Chim. Acta* **2011**, *372*, 145.

[86] S. Kumari, A. K. Mahato, A. Maurya, V. K. Singh, N. Kesharwani, P. Kachhap, I. O. Koshevoy, C. Haldar, *New J. Chem.* **2017**, *41*, 13625.

[87] A. Guha, T. Chattopadhyay, N. D. Paul, M. Mukherjee, S. Goswami, T. K. Mondal, E. Zangrando, D. Das, *Inorg. Chem.* **2012**, *51*, 8750.

[88] A. K. Dhara, U. P. Singh, K. Ghosh, *Inorg. Chem. Front.* **2016**, *3*, 1543.

[89] S. K. Mal, M. Mitra, C. S. Purohit, R. Ghosh, *Polyhedron* **2015**, *101*, 191.

[90] a) T. Ghosh, J. Adhikary, P. Chakraborty, P. K. Sukul, M. S. Jana, T. K. Mondal, E. Zangrando, D. Das, *Dalton Trans.* **2014**, *43*, 841. b) B. J. Hathaway, G. Wilkinsons, R. G. Gillard, J. A. McCleverty, *Comprehensive Coordination Chemistry*, Vol. 5, Pergamon Press, Oxford, **1987**, 861. c) U. Sakaguchi, A. W. Addison, *J. Chem. Soc., Dalton.Trans.* **1979**, 600. d) M. Palaniandavar, I. Somasundaram, M. Lakshminarayanan, H. Manohar, *J. Chem. Soc. Dalton Trans.* **1996**, 1333. e) M. Murali, M. Palaniandavar, T. Pandiyan, *Inorg. Chim. Acta* **1994**, *224*, 19.

[91] J. C. Mills, N. L. Stone, J. Erhardt, R. N. Pittman, *J. Cell Biol.* **1998**, *140*, 627.

[92] N. R. Filipovíc, S. Bjelogrlíc, A. Marinkovíc, T. Ž. Verbíc, I. N. Cvijetiíc, M. Sećanski, M. Rodíc, M. Vujcíc, D. Sladíc, Z. Strikovíc, T. R. Todorovíc, C. D. Muller, *RSC Adv.* **2015**, *5*, 95191.

[93] J. Qian, W. Gu, H. Liu, F. X. Gao, L. Feng, S. P. Yan, D. Z. Liao, P. Cheng, *Dalton Trans.* **2007**, 1060.

[94] M. Niu, Z. Li, H. Li, X. Li, J. Dou, S. Wang, *RSC Adv.* **2015**, *5*, 37085.

[95] C.-Y. Gao, X. Qiao, Z. –. Y. Ma, Z.-G. Wang, J. Lu, J.-L. Tian, J.-Y. Xu, S.-P. Yan, *Dalton Trans.* **2012**, *41*, 12220.

[96] R. W. Y. Sun, A. L. F. Chow, X. H. Li, J. J. Yan, S. S. Y. Chui, *Chem. Sci.* **2011**, *2*, 728.

[97] R. Buchtík, Z. Trávníček, J. Vančo, R. Herchel, Z. Dvořák, *Dalton Trans.* **2011**, *40*, 9404.

SUPPORTING INFORMATION

Additional supporting information may be found online in the Supporting Information section at the end of the article.

How to cite this article: Mondal SS, Chatterjee M, Tiwari RK, et al. Hexanuclear Zn(II) and Mononuclear Cu(II) Complexes containing imino phenol ligands: Exploitation of their Catalytic and Biological Perspectives. *Appl Organometal Chem*. 2019;e5011. https://doi.org/10.1002/aoc.5011